the plant journal

SEB SOCIETY FOR EXPERIMENTAL BIOLOGY

The Plant Journal (2024) **120,** 218–233 doi: 10.1111/tpj.16982

Phosphate deficiency alters transcript isoforms via alternative transcription start sites

Rodrigo S. Reis[1,2], Joaquín Clúa[1], Aime Jaskolowski[1], Jules Deforges[1], Dominique Jacques-Vuarambon[1,2], Nicolas Guex[3] and Yves Poirier[1,*]

[1]*Department of Plant Molecular Biology, University of Lausanne, Biophore Building, Lausanne CH-1015, Switzerland,*
[2]*Institute of Plant Sciences, University of Bern, Bern CH-3013, Switzerland, and*
[3]*Bioinfomatics Competence Center, University of Lausanne, Lausanne, Switzerland*

Received 13 November 2023; revised 24 May 2024; accepted 13 July 2024; published online 20 August 2024.
*For correspondence (e-mail yves.poirier@unil.ch).

SUMMARY

Alternative transcription start sites (TSS) are widespread in eukaryotes and can alter the 5′ UTR length and coding potential of transcripts. Here we show that inorganic phosphate (Pi) availability regulates the usage of several alternative TSS in Arabidopsis (*Arabidopsis thaliana*). In comparison to phytohormone treatment, Pi had a pronounced and specific effect on the usage of many alternative TSS. By combining short-read RNA sequencing with long-read sequencing of full-length mRNAs, we identified a set of 45 genes showing alternative TSS under Pi deficiency. Alternative TSS affected several processes, such as translation via the exclusion of upstream open reading frames present in the 5′ UTR of *RETICULAN LIKE PROTEIN B1* mRNA, and subcellular localization via removal of the plastid transit peptide coding region from the mRNAs of *HEME OXYGENASE 1* and *SULFOQUINOVOSYLDIACYLGLYCEROL 2*. Several alternative TSS also generated shorter transcripts lacking the coding potential for important domains. For example, the *EVOLUTIONARILY CONSERVED C-TERMINAL REGION 4* (*ECT4*) locus, which encodes an N^6-methyladenosine (m^6A) reader, strongly expressed under Pi deficiency a short noncoding transcript (named ALT_{ECT4}) ~550 nt long with a TSS in the penultimate intron. The specific and robust induction of ALT_{ECT4} production by Pi deficiency led to the identification of a role for m^6A readers in primary root growth in response to low phosphate that is dependent on iron and is involved in modulating cell division in the root meristem. Our results identify alternative TSS usage as an important process in the plant response to Pi deficiency.

Keywords: ECT4, noncoding RNA, phosphate deficiency, transcription start sites, upstream open reading frame.

INTRODUCTION

Alternative transcription start site (TSS) usage is an important regulatory mechanism altering mRNA and protein diversity (de Klerk & 't Hoen, 2015; Forrest et al., 2014; Kurihara et al., 2018; Ushijima et al., 2017; Wang et al., 2019). In humans, an average of four different TSS are expressed per gene, many exhibiting tight tissue- or cell-type-specific regulation (de Klerk & 't Hoen, 2015; Forrest et al., 2014). Indeed, alternative transcription initiation and termination, rather than alternative splicing, are the main drivers of transcript isoform diversity in humans (Reyes & Huber, 2018). Alternative TSS usage is also common in plants, with a recent study identifying more than 2000 genes in Arabidopsis (*Arabidopsis thaliana*) containing alternative TSS that were more than 100 bp apart (Zhang et al., 2022). Alternative TSS can affect the presence of regulatory elements found in the 5′ UTRs of mRNAs, often fine-tuning translation. For instance, blue light induces downstream TSS usage in two key light-inducible transcription factor genes, *HY5* and *HYH*, producing shorter transcripts with higher translation efficiency, as they lack inhibitory upstream open reading frames (uORFs) (Kurihara et al., 2018). In many cases, alternative TSS usage produces shorter protein sequences that display differential elements within their N-termini, including transit peptides. Such isoforms play an important role in light-dependent changes in the subcellular localization of proteins, such as GLYCERATE KINASE (GLYK) (Ushijima et al., 2017). GLYK functions as a photorespiration enzyme in chloroplasts; however, shade induces the expression of an isoform that lacks the chloroplast signal peptide and is thus retained in the cytoplasm, a process that plays an important role in plant adaptation to light

fluctuations. Alternative TSS usage can also produce transcript isoforms that are significantly shorter than the annotated reference isoforms (Forrest et al., 2014; Wang et al., 2019), with many that are likely too short to encode for functional proteins. However, the functions of noncoding transcript isoforms originating from alternative TSS usage are poorly characterized.

Phosphorus (P) is one of the most important elements limiting plant growth, in large part because it is poorly assimilated from the soil due to the presence of insoluble complexes of P with calcium as well as oxides and hydroxides of iron and aluminum (Roy et al., 2016). High crop yield is thus often attained through the use of fertilizers containing large amounts of soluble inorganic orthophosphate (Pi). Unfortunately, Pi obtained from the mining and transformation of phosphate rock is a non-renewable resource, with a major impact on the environment (Sattari et al., 2016). Hence, there is an increasingly urgent need to improve plant Pi acquisition and usage to enable the lower use of fertilizers with minimum impacts on crop yield. Pi deficiency leads to broad changes in gene expression and associated metabolic and physiological adaptive changes in plants to optimize Pi acquisition and use (Poirier et al., 2022), including changes in root architecture (Gutiérrez-Alanís et al., 2018) and the secretion of organic acids and enzymes in the root apoplast to optimize Pi acquisition (Zhang et al., 2014). Consequently, Pi homeostasis is tightly regulated by various molecular mechanisms, from the transcriptional to post-translational levels (Gutiérrez-Alanís et al., 2018; Ham et al., 2018; Jung et al., 2018).

Genome-wide transcriptomic analysis has revealed numerous protein-coding genes, as well as long noncoding RNAs and small regulatory RNAs, that are transcriptionally regulated by Pi deficiency (Bazin et al., 2017; Hsieh et al., 2010; Misson et al., 2005). Such studies have uncovered numerous genes with key roles in the adaptation of plants to Pi deficiency, such as genes involved in lipid remodeling (Cruz-Ramírez et al., 2006), the small RNA miR399 and its noncoding target mimic IPS1 (Franco-Zorrilla et al., 2007), as well as several *cis*- and *trans*-natural antisense transcripts affecting mRNA translation (Deforges, Reis, Jacquet, Sheppard, et al., 2019; Deforges, Reis, Jacquet, Vuarambon, et al., 2019; Reis et al., 2020). Analysis of transcriptomic data also revealed an important role for alternative splicing in the adaptation of plants to Pi deficiency (Dong et al., 2018; Li et al., 2013; Tian et al., 2021), including the alternative splicing of *REGULATOR OF LEAF INCLINATION* (*RLI1*) in the control of leaf growth in rice (*Oryza sativa*) (Guo et al., 2022). Whereas identifying alternative TSS has the potential to uncover genes involved in the adaptation of plants to the environment (Kurihara et al., 2018; Ushijima et al., 2017), the contribution of alternative TSS to the response of plants to Pi deficiency is unknown.

Here, we studied the alternative TSS usage landscape induced by Pi deficiency in Arabidopsis. We identified several Pi-specific alternative transcripts, including shorter transcripts lacking uORFs and other putative inhibitory elements, as well as transit peptide sequences. Several of the proteins encoded by the identified shorter transcripts lacked (either partially or fully) their functional domain(s). Among these, the N^6-methyladenosine (m^6A) reader gene *EVOLUTIONARILY CONSERVED C-TERMINUS 4* (*ECT4*) expressed a short isoform (ALT_{ECT4}) specifically in response to Pi starvation. The ALT_{ECT4} transcript is likely non-coding, with no conserved coding sequence and lacking a functional domain. A higher-order null mutant for the major m^6A readers in Arabidopsis (i.e., the *ect2 ect3 ect4* triple mutant) was affected in primary root growth under Pi deficiency, a process that involves the modulation of meristematic zone size based on the presence of iron, thus revealing an important role for the m^6A RNA modification pathway in root development and Pi homeostasis.

RESULTS AND DISCUSSION

Phosphate deficiency regulates alternative TSS usage

To identify transcripts with alternative TSS induced specifically by Pi deficiency, we performed JunctionSeq (Hartley & Mullikin, 2016) of our previously published short-read RNA sequencing dataset (Deforges, Reis, Jacquet, Sheppard, et al., 2019) from Arabidopsis grown in liquid culture in the presence of a high (1 mM) or low (100 μM) Pi concentration, as well as roots and shoots from seedlings grown on agar-solidified medium supplemented with different phytohormones, including auxin (indole acetic acid [IAA]), abscisic acid (ABA), methyl-jasmonate (MeJA), or the ethylene precursor 1-aminocyclopropane-1-carboxylic acid (Figure 1A). We used JunctionSeq to identify the differential usage of exonic regions only; splice junctions were not considered, and intron retention was not calculated. Consequently, only alternative TSS transcripts encompassing at least one exon in the corresponding reference gene locus were analyzed. This approach identified 294 genes with differential exonic regions associated with Pi deficiency, 259 (88%) of which were specific to the Pi treatment dataset (Figure 1B; Data S1). We also identified 324 genes with differential exonic expression specific to either roots or shoots under standard growth conditions, suggesting that organ identity might involve differential TSS usage.

Next, we used the same RNA samples obtained from Arabidopsis grown in high- and low-Pi media (Deforges, Reis, Jacquet, Sheppard, et al., 2019) to analyze full-length, capped, polyadenylated RNA using TeloPrime cDNA synthesis (Cartolano et al., 2016) followed by PacBio long-read sequencing (Figure 1A). Whereas this approach has the advantage of analyzing full-length transcripts and is not constrained by genomic features (e.g., exonic regions), it is

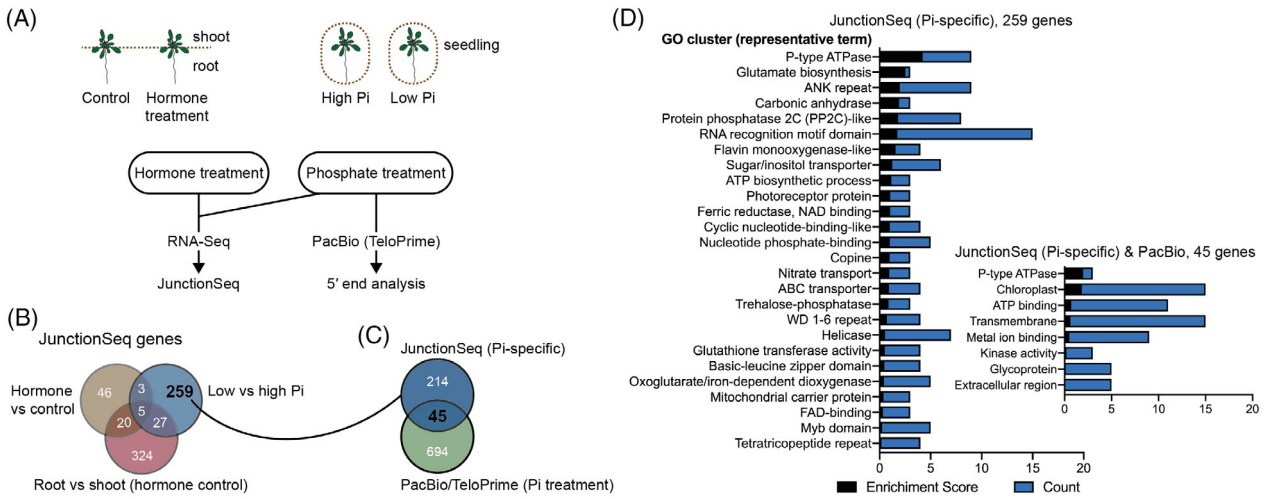

Figure 1. Pi deficiency regulates genome-wide alternative transcription start site (TSS).
(A) Experimental design for alternative TSS identification. Total RNA was extracted from the roots and shoots of phytohormone-treated 10-day-old seedlings grown on solid Murashige and Skoog (MS) medium and 7-day-old seedlings grown in Pi-deficient (100 μM versus the standard 1 mM Pi) liquid MS medium. RNA-Seq data were produced for all samples and analyzed using JunctionSeq. PacBio long-read data were produced from full-length cDNA samples (TeloPrime) of Pi-sufficient and Pi-deficient plants.
(B) Venn diagram showing the number of significant differentially expressed genes ($P < 0.01$) in the JunctionSeq data.
(C) Venn diagram showing the number of significant differentially expressed genes in the Pi-specific JunctionSeq ($P < 0.01$) and PacBio ($P < 0.05$ for 5′ UTRs and $P < 0.1$ for coding regions) data.
(D) Gene ontology (GO) analysis of the Pi-specific JunctionSeq dataset. GO analysis of Pi-specific genes in the overlap between JunctionSeq and PacBio data is shown in the inset.

limited by its lower coverage depth. Therefore, in the first analysis, we used low threshold criteria to identify potential alternative TSS, defined as transcripts displaying different 5′ ends within either the 5′ UTR (chi-squared test; *P* value <0.05) or the coding region (chi-squared test; *P* value <0.1) compared to the longest annotated full-length transcript. From this low-threshold analysis, 739 unique genes were associated with at least one instance of differential TSS usage between high- and low-Pi samples. We then leveraged both approaches to identify higher-confidence, Pi-specific genes that are associated with differential TSS usage, resulting in a set of 45 genes identified by both JunctionSeq and PacBio analyses (Figure 1C; Data S1). Evidence of transcription from alternative TSSs similar to most of these 45 genes has been reported in large-scale TSS analysis (Nielsen et al., 2019); however, few of them have been identified in condition-specific studies, such as cold (Kindgren et al., 2018) and light response (Kurihara et al., 2018; Ushijima et al., 2017) (Figure S1).

To gain insights into the possible roles of the identified genes associated with differential TSS usage specific to Pi starvation, we first performed a gene ontology (GO) enrichment analysis using the 259 Pi-specific JunctionSeq genes (Figure 1B). The most highly enriched GO terms were associated with energetic and metabolic processes, while RNA recognition motif domain was the most abundant term (Figure 1D). We then performed GO enrichment analysis using the 45 genes identified by both JunctionSeq and PacBio analyses. Terms associated with energetic processes showed the highest enrichment scores, while chloroplast and transmembrane were the most abundant terms (Figure 1D, inset). Altogether, our analyses revealed 45 high-confidence, Pi-starvation-specific genes associated with alternative TSS usage that are potentially involved in processes such as energy balance and processes occurring in the chloroplast.

Presence of uORF regulated by differential usage of alternative TSS

The presence of a uORF is a common feature of the 5′ UTRs of mRNAs in Arabidopsis; uORFs often function as translation inhibitors of the related main ORF (mORF) (Ebina et al., 2015; Kurihara et al., 2018). Here, we observed that genes associated with alternative TSS usage were enriched for the presence of uORFs in our datasets (Data S1). Approximately 70% of genes in the Pi-specific JunctionSeq (186/259) and PacBio (343/495; differential uORF analysis) datasets contained at least one uORF in their 5′ UTRs, whereas ~75% (24/31) contained at least one uORF among the subset of Pi-specific genes identified in both analyses. The latter dataset corresponds to a subset of the 45 high-confidence Pi starvation-specific genes (described above) in which only genes displaying differential TSS usage within their 5′ UTR were considered. uORFs that are translated are more likely to have inhibitory effect on translation of the main ORF and a recent work reported

high-depth analysis of uORF translation (Wu et al., 2024). Using this published dataset, we compared the presence of translated uORF in genes identified in our selected datasets with that of translated uORF in randomly selected Arabidopsis gene lists of corresponding size (Data S1) present in the Wu et al. (2024) dataset and in our transcriptome. The number of translated uORFs in our JunctionSeq_Pi (49/259), PacBio (51/495) and overlapping (10/31) datasets is significantly higher (Fisher's exact test; average *P*-value from 1000 iterations) than that in random gene lists, indicating that genes with differential TSS usage in Pi starvation are enriched for the presence of translated uORFs (Figure 2A).

Translation inhibition of the mORF by an uORF in the 5′ UTR has been observed for several transcripts (Ebina et al., 2015; Kurihara et al., 2018; Srivastava et al., 2018), with potential effects on plant development and adaptation. For example, translational inhibition of *PHOSPHATE1* (*PHO1*) by a uORF regulates rosette growth under low phosphate levels (Reis et al., 2020). Here, among the genes harboring uORFs identified by both JunctionSeq and PacBio analysis, we observed that Pi deficiency induced the expression of a longer *RETICULAN-LIKE PROTEIN B1* (*RTNLB1*; *AT4G23630*) transcript harboring nine uORFs (ranging from 21 to ~144 nucleotides long) within its 5′ UTR. Strikingly, all nine uORFs were absent from the shorter, alternative *RTNLB1* (ALT_{RTNLB1}) transcript (Figure 2B; Figure S2a; Table S1). In this analysis, we used as our reference transcript the *RTNLB1* transcript annotated in Araport11 (Cheng et al., 2017), which is the longer mRNA harboring nine uORFs that was not detected under our control conditions. Arabidopsis contains 21 *RTNLB* genes (Nziengui et al., 2007) encoding proteins that help confer curvature to the endoplasmic reticulum (ER) and are required for regulating the transport of newly synthesized FLAGELLIN SENSITIVE2 (FLS2) from the ER to the plasma membrane (RTNLB1 and RTNLB2) (Lee et al., 2011) and the formation of primary plasmodesmata (RTNLB3 and RTNLB6) (Knox et al., 2015).

To investigate the possible regulatory role of uORFs in *RTNLB1* mRNA, the *RTNLB1* short (i.e., ALT_{RTNLB1}) 5′ UTR, the long (i.e., *RTNLB1*) 5′ UTR as well as a mutated version of the long 5′ UTR (*RTNLB1* Δ*uORF*) where all nine ATG codons of the uORFs were mutated to ATT (Table S1), were independently fused to the *Nano Luciferase* gene and the luminescence levels of the various constructs were compared in transfected protoplasts. The fusion of the *Nano Luciferase* gene to the ALT_{RTNLB1} and the *RTNLB1* Δ*uORF* 5′ UTRs resulted in similar luminescence level which was sixfold higher compared to fusion to the *RTNLB1* 5′ UTR (Figure 2C), indicating that the long *RTNLB1* 5′ UTR (expressed only under low-Pi conditions) harbors uORFs inhibiting the translation of *RTNLB1*. These

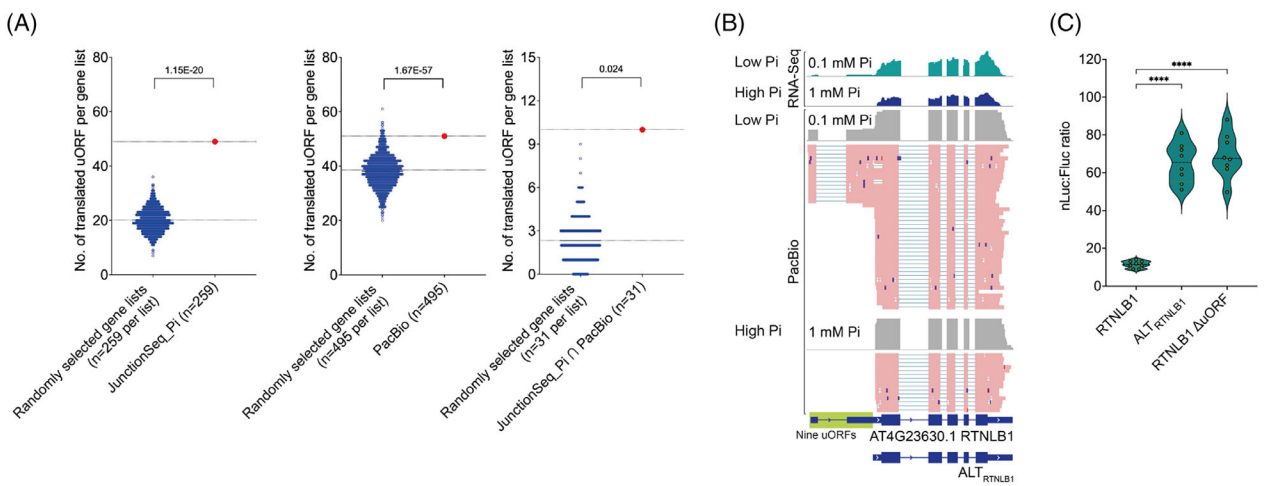

Figure 2. Presence of upstream open reading frame (uORF) in Pi-modulated alternative transcription start site (TSS) isoforms.
(A) Distribution of randomly selected Arabidopsis genes present in the transcriptome and harboring translated uORFs, as reported by Wu et al. (2024), is plotted and compared to the frequency of translated uORFs in genes found in the JunctionSeq_Pi and PacBio datasets, as well as in their overlap. Randomly selected gene lists of corresponding size to each dataset were drawn 1000 times for comparison and the *P*-value was calculated as the average *P*-value (Fisher's exact test, $P < 0.05$) of all comparisons.
(B) RNA-Seq and PacBio reads for *RTNLB1* (AT4G23630) locus in Pi-deficient plants. ALT_{RTNLB1} sequence is depicted using *RTNLB1*'s annotation for its coding sequence (thickest line; bottom panel). Exons are depicted as larger filled boxes, 5′ and 3′ UTRs as thinner filled boxes and introns as lines in the bottom panel, with the direction of transcript indicated by arrowheads.
(C) Effects of variant 5′ UTRs present in *RTNLB1* transcripts on the synthesis of Nano Luciferase in transiently transformed Arabidopsis protoplasts. Comparison is made between constructs harboring the long *RTNLB1* 5′ UTR, the short 5′ UTR associated with the alternative transcript ALT_{RTNLB1}, and a mutated version of the *RTNLB1* 5′ UTR with all nine uORF's ATG codons mutated to ATT (*RTNLB1* ΔuORF). Normalized luminescence (nLUC:Fluc ratio) is the nano luciferase (nLuc) luminescence normalized to the firefly luciferase (Fluc) luminescence expressed from the same plasmid ($n = 8$ biological replicates; one-way ANOVA, ****$P < 0.0001$).

data indicate that the low-Pi-induced expression of the long *RTNLB1* transcript containing nine uORFs in its 5′ UTR likely down-regulates RTNLB1 protein levels. Phosphate deficiency induces ER-stress-dependent autophagy (Naumann et al., 2019). Since reticulon proteins are involved in ER autophagy in maize (*Zea mays*) endosperm (Zhang et al., 2020), it would be interesting to examine the potential contribution of RTNLB1 to Pi-deficiency-induced ER autophagy. Altogether, our results indicate that uORFs are enriched in genes with differential TSS usage under Pi starvation and that the modulation of uORF presence plays a role in regulating the plant response to Pi starvation.

Differential usage of alternative TSS leads to the depletion of transit peptides

Signal and transit peptides are short, typically N-terminal amino acid sequences that target proteins through the secretory pathway or to various organelles, respectively, in eukaryotes (Teufel et al., 2022). Shorter transcripts encoding proteins with disrupted signal or transit peptide sequences might thus display altered subcellular localizations. We predicted signal or transit peptide sequences for 18 of the 45 high-confidence, Pi-specific proteins associated with differential TSS usage, including HEME OXYGENASE 1 (HY1; AT2G26670) and SULFOQUINOVOSYLDIACYLGLYCEROL 2 (SQD2; AT5G01220; Figure 3A,B; Data S1).

HY1 (also named HO1) is a plastidial enzyme that catalyzes the oxygenation of heme to biliverdin Ixα, the precursor of the phytochrome chromophore (Davis et al., 1999). The oxygenation reaction also generates carbon monoxide and free iron. Analysis of *HY1* transcripts by PacBio revealed the presence of alternative TSS that would lead to the production of a truncated protein without the transit peptide. Whereas under Pi-sufficient conditions, 86% (24 out of 28) of *HY1* transcripts encoded a functional transit peptide, only 22% of *HY1* transcripts (16 out of 72) under Pi-deficient condition encoded a full-length protein with a transit peptide (Figure 3A). These results indicate that the majority of HY1 protein synthesized under Pi-deficient conditions would likely remain in the cytosol. The Arabidopsis genome encodes three other HY1 homologous proteins (HO2-HO4), which all contain a plastidial transit peptide at the N-terminus (Emborg et al., 2006). Beyond phytochrome biosynthesis, HY1 functions in plant responses to stress conditions that generate reactive oxygen species (ROS), such as treatment with high salt, cadmium, or boron, as well as UV and drought (Shekhawat & Verma, 2010). Notably, the catalytic products biliverdin IX and carbon monoxide themselves function in antioxidant defense mediated by HY1 (Mahawar & Shekhawat, 2018). It would be interesting to examine whether a cytosolic variant of HY1 functions in plant defense against ROS generated during Pi deficiency stress.

The Arabidopsis genome contains a single *SQD2* gene encoding a plastidial enzyme involved in the synthesis of sulfolipids (Yu et al., 2002). *SQD2* expression is known to robustly increase under Pi deficiency, a stress that results in the replacement of phospholipids with sulfo- and galactolipids (Essigmann et al., 1998). In agreement, PacBio data showed a nearly 18-fold increase in *SQD2* transcripts under Pi deficiency (Figure 3B). Interestingly, PacBio data also showed that several alternative TSS were used in *SQD2* transcription under both Pi-sufficient and Pi-deficient conditions, with shorter transcripts resulting in proteins with truncated or deleted plastidial transit peptides (Figure 3B). Under Pi-deficient condition, while the longer *SQD2* transcripts encoding a protein that included the N-terminal plastidial transit peptide increased fivefold (from 10 to 50 transcripts) relative to the Pi-sufficient condition, the truncated *SQD2* transcripts increased by approximately 29-fold (from 11 to 323 transcripts) under the same condition. Thus, while Pi deficiency results in an increase in transcripts encoding plastidial SQD2, the increase in transcript encoding a potentially cytosolic variant of SQD2 is even stronger. The rice genome contains three *SQD2* genes, with *SQD2.1* encoding a plastidial protein and both *SQD2.2* and *SQD2.3* encoding cytosolic variants (Zhan et al., 2019). Notably, SQD2.1 has dual activities, as it catalyzes not only sulfoquinovosyldiacylglycerol biosynthesis but also flavonoid glycosylation, particularly the synthesis of apigenin-7-*O*-glucoside (A7G), whereas cytosolic SQD2.2 is only involved in A7G synthesis (Zhan et al., 2017, 2019). A7G accumulation in both plastids and the cytosol participates in ROS scavenging under various stresses, such as salinity and drought stress (Zhan et al., 2019). The observed stronger increase in synthesis of the shorter *SQD2* transcripts encoding a protein devoid of functional transit peptide in Arabidopsis grown under Pi-deficient conditions could thus represent a mechanism to increase the synthesis of cytosolic A7G under such nutrient stress, which is also known to be associated with increased ROS production (Tarkowski et al., 2023).

A study of phytochrome-mediated alternative promoter selection using the *phyA phyB* mutant and red-light treatment identified 2104 genes associated with alternative TSS, 397 (19%) of which were predicted to encode proteins with different subcellular localizations (Ushijima et al., 2017). Notably, *HY1* and *SQD2* were not among these 397 genes. By contrast, 18 out of 45 high-confidence genes (40%) associated with alternative TSS in plants under Pi starvation showed altered signal or transit peptide production. Altogether, these results suggest that alternative TSS selection is a common strategy to alter the subcellular localization of proteins in response to environmental cues.

Differential usage of alternative TSS may lead to noncoding RNA expression

Although alternative TSS usage plays important roles in regulating gene expression and protein localization, much less is known about its role in generating noncoding RNAs. We

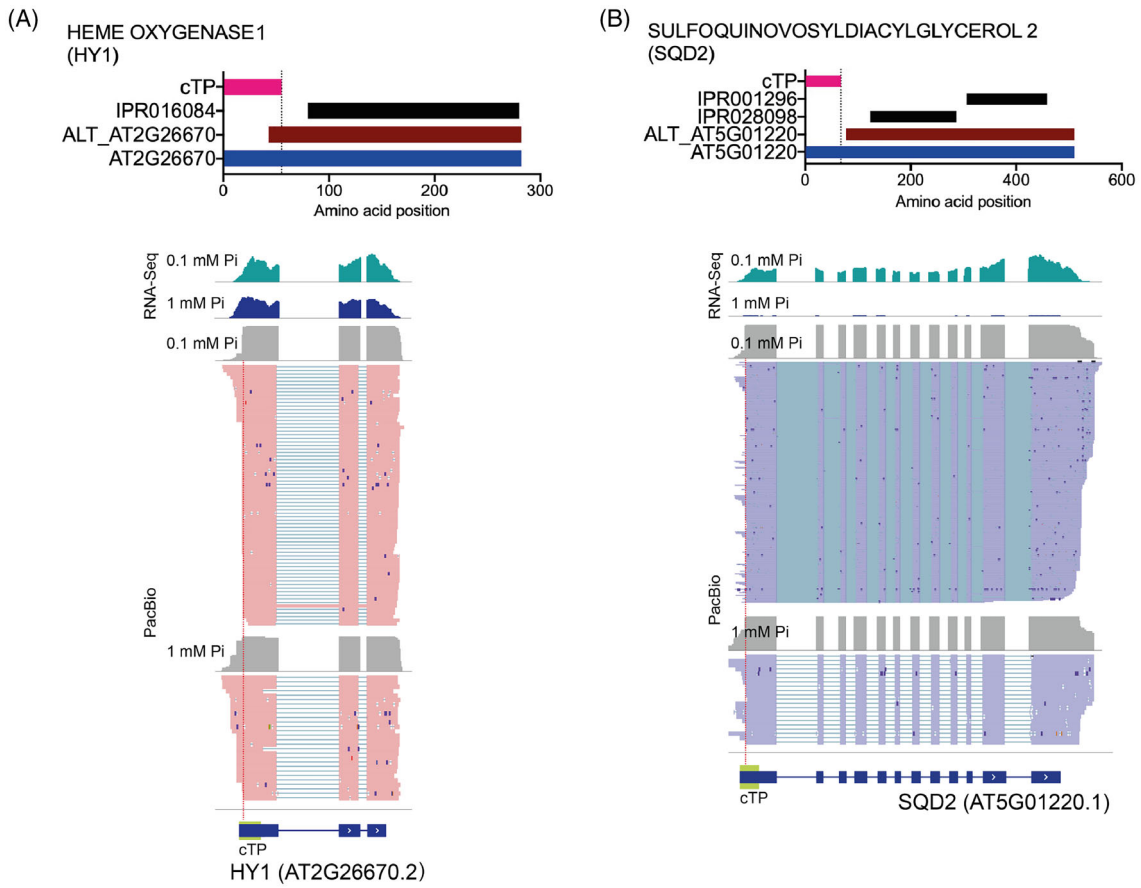

Figure 3. Pi-modulated alternative transcription start site (TSS) isoforms lack transit peptide sequences.
(A, B) Upper panels, amino acid positions of the plastid transit peptide (cTP, pink bars), predicted domains (black bars), alternative-isoform-encoded protein (brown bars), and reference protein (blue bars) for HY1 (A) and SQD2 (B). Alternative-isoform-encoded amino acid sequence was defined as the longest open reading frame ending at the reference transcript's STOP codon, i.e., exhibiting the same (complete or partial) amino acid sequence as that found in the reference protein. Lower panels, RNA-Seq and PacBio reads for the *HY1* (A) and *SQD2* (B) loci in plants under Pi-sufficient and Pi-deficient conditions, with the region encoding the transit peptide highlighted in yellow-green (UTRs are not depicted in the gene model diagram).

could predict protein domains for 36 out of 259 genes identified in Pi-specific JunctionSeq analysis using InterProScan5 (Jones et al., 2014), including 10 genes corroborated by PacBio analysis (Data S1). We observed that 16 genes with shorter mRNA isoforms in Pi-specific JunctionSeq dataset (six also in PacBio dataset) either fully or partially lacked sequences encoding for at least one functional domain(s), while 22 genes (five also in PacBio dataset) had at least one complete domain sequence (Figure 4A). Shorter isoforms of some transcripts lacked any complete domain (Figure 4B), including *EVOLUTIONARILY CONSERVED C-TERMINAL REGION 4* (*ECT4*; AT1G55500), *HARMLESS TO OZONE LAYER 2* (*HOL2*; AT2G43920), *CYCLIN-DEPENDANT KINASE GROUP C2* (*CDKC2*; AT5G64960), and *AT3G33530* (Figure 4C–E; Figure S2b,c). The shorter transcript isoform of *HOL2* that we identified has been annotated in Araport11 (Cheng et al., 2017) and encodes a protein with a truncated functional domain (*S*-adenosyl-L-methionine-dependent methyltransferase), thus potentially producing a protein with different properties from the longer *HOL2* transcript. On the other hand, the shorter isoform of *CDKC2*, which has not been annotated in Araport11, does not encode a protein with a kinase domain. The shorter isoform of *ECT4* (ALT_{ECT4}), also not annotated in Araport11, does not contain any ORF in frame with the reference sequence for *ECT4*, suggesting that it is a *bona fide* noncoding RNA. Similar disruption or exclusion of functional domains via differential TSS usage was recently described during pathogen-associated molecular pattern-triggered immunity (Thieffry et al., 2022). The existence of short isoforms lacking functional domains is intriguing because it suggests the possibility of transcript repurposing (from coding to noncoding) via alternative TSS usage.

Pi deficiency induces strong and specific expression of an alternative promoter associated with an m^{6}A reader

Next, we investigated alternative TSS usage at the *ECT4* locus in detail. *ECT4* encodes a protein containing a highly

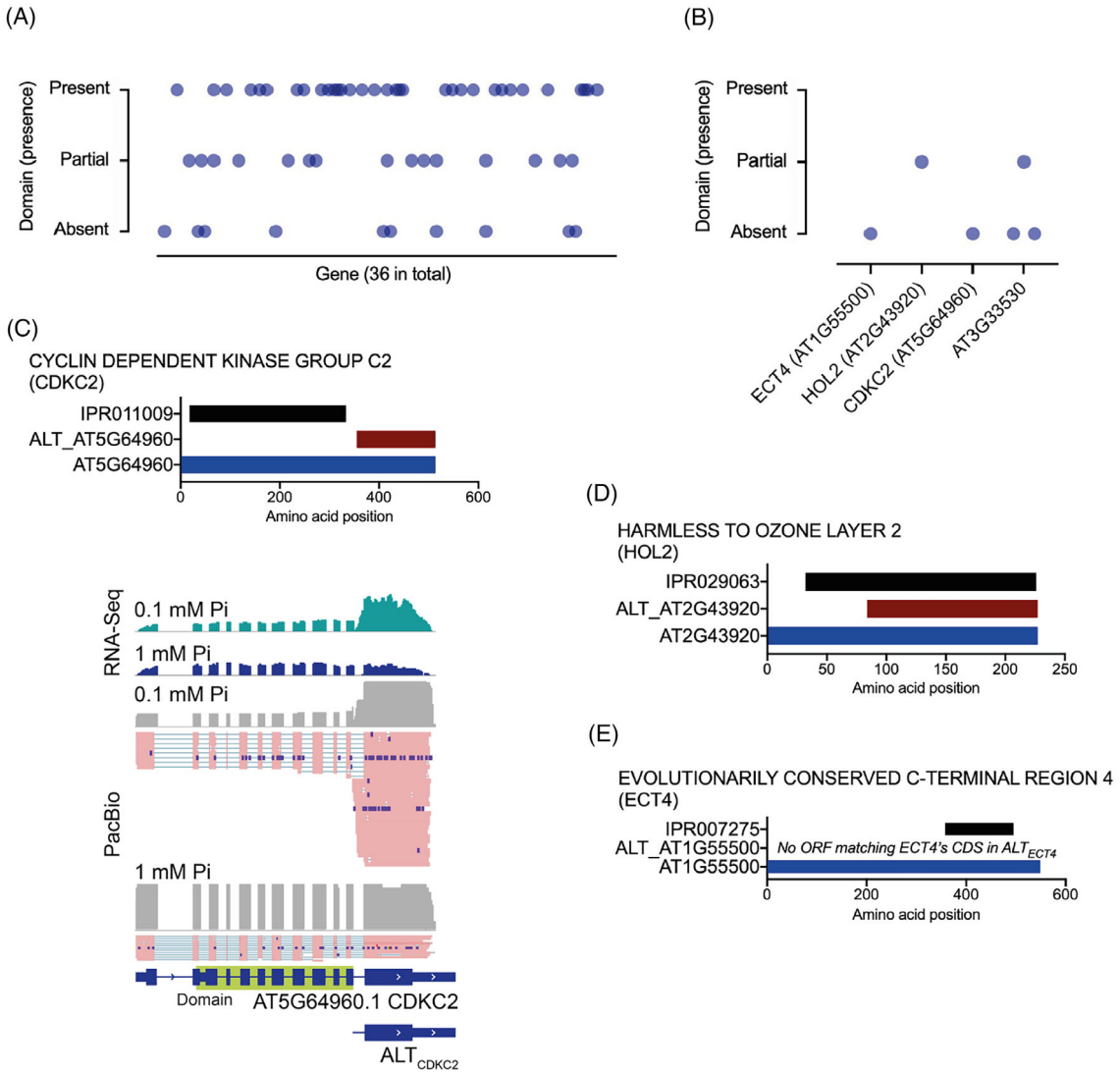

Figure 4. Alternative transcription start site (TSS) isoforms generate transcripts lacking functional domains.
(A, B) Presence of predicted domains for proteins encoded in Pi-specific JunctionSeq dataset, i.e., total of 36 genes with one or more predicted domain, where 10 are corroborated by the PacBio analysis (Data S1). Entire domain is present ("present"), domain portion is present ("partial"), or domain is completely absent ("absent"). (B) Same as (A), but only genes with only partial or absent domain were plotted.
(C–E) Amino acid positions of the predicted domain (black bar), alternative-isoform-encoded protein (brown bar), and reference protein (blue bar). Alternative-isoform-encoded amino acid sequence was defined as the longest open reading frame ending at the reference transcript's STOP codon, i.e., exhibiting the same (complete or partial) amino acid sequence as that found in the reference protein. RNA-Seq and PacBio reads for the *CDKC2* (AT5G64960) locus in Pi-sufficient and Pi-deficient plants [(C) bottom panel]. Exons are depicted as larger filled boxes, 5′ and 3′ UTRs as thinner filled boxes, and introns as lines in the bottom panel, with the direction of transcription indicated by arrows.

conserved YT521-B homology (YTH) domain (InterPro IPR007275) involved in binding N^6-methyladenosine (m^6A) in mRNAs. m^6A, the most abundant internal modification of mRNAs in eukaryotes, affects numerous aspects of mRNA metabolism, including secondary structure, stability, and translation (Prall et al., 2023). m^6A modification is reversible and requires the actions of m^6A methyltransferases, demethylases, and readers to deposit, remove, and interpret, respectively, m^6A on mRNAs. The modification of mRNAs by m^6A affects numerous aspects of plant development and responses to various stresses (Arribas-Hernández et al., 2018; Shao et al., 2021). The Arabidopsis genome contains 13 genes encoding proteins with an YTH domain that are collectively referred to as "m^6A readers": *ECT* (*ECT1-11*), *CPS30L*, and *YTH11* (Li et al., 2014). In Arabidopsis, ECT2, ECT3, and ECT4 play largely redundant roles in leaf growth and organogenesis (Arribas-Hernández et al., 2018, 2020), as well as in ABA responses during seed germination and post-germination growth (Song et al., 2023). At the molecular level, this

redundancy is reflected by the ability of ECT2, ECT3, and ECT4 to bind to and stabilize overlapping sets of m^{6}A-modified mRNAs (Arribas-Hernández et al., 2021; Song et al., 2023).

Under Pi deficiency, the *ECT4* locus transcribes an alternative transcript, ALT_{ECT4}, which is initiated within the seventh intron of *ECT4*, producing a 2-exon transcript of ~550 nucleotides comprising *ECT4* exons 8 and 9 and thus lacking the YTH domain (Figure 5A). We identified five short ORFs within the ALT_{ECT4} transcript, but none were in frame with the full-length *ECT4* CDS, suggesting that ALT_{ECT4} either is a noncoding RNA or encodes an ECT4-unrelated peptide(s) that is not conserved in other plants (Table S2). ALT_{ECT4} expression was strongly and specifically induced by phosphate deficiency (Data S1; Figure S2c). In addition to being unaffected by hormone treatment (Figure S2c), ALT_{ECT4} expression was also unaffected by nitrogen deficiency (Figure S3). Reverse transcription–quantitative PCR (RT–qPCR) showed that Pi starvation enhanced ALT_{ECT4} expression in roots and shoots and that its expression increased at 7 days post-germination, reaching its highest levels in roots after 10–12 days of treatment (Figure 5B). Consistent with our RNA sequencing data, full-length *ECT4* expression was only slightly induced by Pi deficiency (Figure 5B).

To further study the expression of ALT_{ECT4}, we transformed plants with a construct lacking the *ECT4* upstream sequences (i.e., without its promoter and 5′ UTR) and including only the *ECT4* genomic coding sequence (with the START codon) fused in frame (STOP codon removed) with *GFP*. *GFP* expression was induced in these transgenic plants under Pi-deficient conditions, while a control line expressing GFP from the CaMV35S promoter maintained strong GFP expression under both Pi-sufficient and Pi-deficient conditions. Together, these data show that the transcription of *GFP* was independent of the *ECT4* promoter and was driven by promoter elements within the genomic coding region of *ECT4* that is responding to Pi-deficiency (hereafter referred to as the ALT_{ECT4} promoter; Figure 5C). Analysis of the *GFP* mRNA by 5′ RACE identified TSS near the 3′ end of exon 7 and within intron 7 of *ECT4*, generating 5′ UTRs of ~320 bp before the start of GFP translation (Table S3).

We then investigated the tissue-specific *ECT4* and ALT_{ECT4} gene expression using promoter-GUS fusions (Figure 5D). The *GUS* expression pattern driven by the *ECT4* promoter was similar in plants grown under Pi-sufficient and Pi-deficient conditions, with broad expression in shoots and strong expression in the root vascular system and the stele region of the root meristem and columella root cap (Figure S4). By contrast, *GUS* expression driven by the ALT_{ECT4} promoter in plants grown under Pi-sufficient conditions was weak at the tip and base of the leaf and cotyledon and undetectable in roots. Under Pi deficiency, ALT_{ECT4}-promoter-driven *GUS* expression was strong throughout the leaf, especially the leaf vasculature, as well as in the vasculature of primary and lateral roots (Figure 5D). Notably, in Pi-deficient plants, *GUS* expression driven by the *ECT4* and ALT_{ECT4} promoters clearly overlapped in leaves and roots. These results demonstrate that ALT_{ECT4} expression is independent of the *ECT4* promoter region and that ALT_{ECT4} promoter is strongly and specifically induced by Pi starvation in tissues where *ECT4* is expressed.

m^{6}A readers modulate primary root growth under phosphate deficiency

The Pi-specific expression of ALT_{ECT4} led us to investigate a potential role for ECT4 and other closely related m^{6}A readers in Pi homeostasis. We analyzed null mutants of *ECT2*, *ECT3*, and *ECT4*, which represent the main clade of m^{6}A readers in Arabidopsis and exhibit genetic redundancy (Arribas-Hernández et al., 2018, 2020; Song et al., 2023). One of the best-described developmental responses of roots to Pi deficiency is the reduction in primary root growth due to reduced root meristem cell division and/or cell elongation (Abel, 2017; Péret et al., 2011). The *ect4* single and *ect2 ect3* double mutants showed wild-type primary root growth under both high- and low-Pi conditions (Figure 6A–C). Although primary root elongation in the *ect2 ect3 ect4* (*te234*) triple mutant was only mildly affected under high-Pi conditions, as previously reported (Arribas-Hernández et al., 2020), root growth in the triple mutant was more strongly inhibited upon Pi deficiency (Figure 6A–D). Importantly, the expression of a *ECT4-Venus* fusion gene construct driven by the *ECT4* native promoter rescued the *te234* mutant phenotype under low-Pi conditions (Figure 6A–C). Analysis of the expression of genes strongly regulated by Pi deficiency in roots, including the noncoding RNA *IPS1*, the galactolipid biosynthetic gene *MGD3*, and the phosphate transporter gene *PHT1;4*, showed similar expression levels in wild-type, *te234*, and *ECT4-Venus* complemented plants (Figure S5). These results suggest that m^{6}A readers play a role in primary root elongation under Pi deficiency without generally perturbing the Pi signaling pathways.

To investigate how Pi starvation inhibits primary root elongation in the *te234* triple mutant, we measured meristem size and cell length in the root differentiation zones of plants under high- and low-Pi conditions. Under high-Pi conditions, meristem size and cell length were similar between *te234* and the wild type (Figure 6E,F). In low Pi, however, *te234* had shorter meristems than the wild type, which was reverted in the triple mutant complemented with ECT4-Venus (Figure 6E). However, cell size in the differentiation zone was unchanged in *te234* compared to the wild type under these conditions (Figure 6F).

Several studies have shown that the reduction in primary root growth under Pi-deficient conditions is

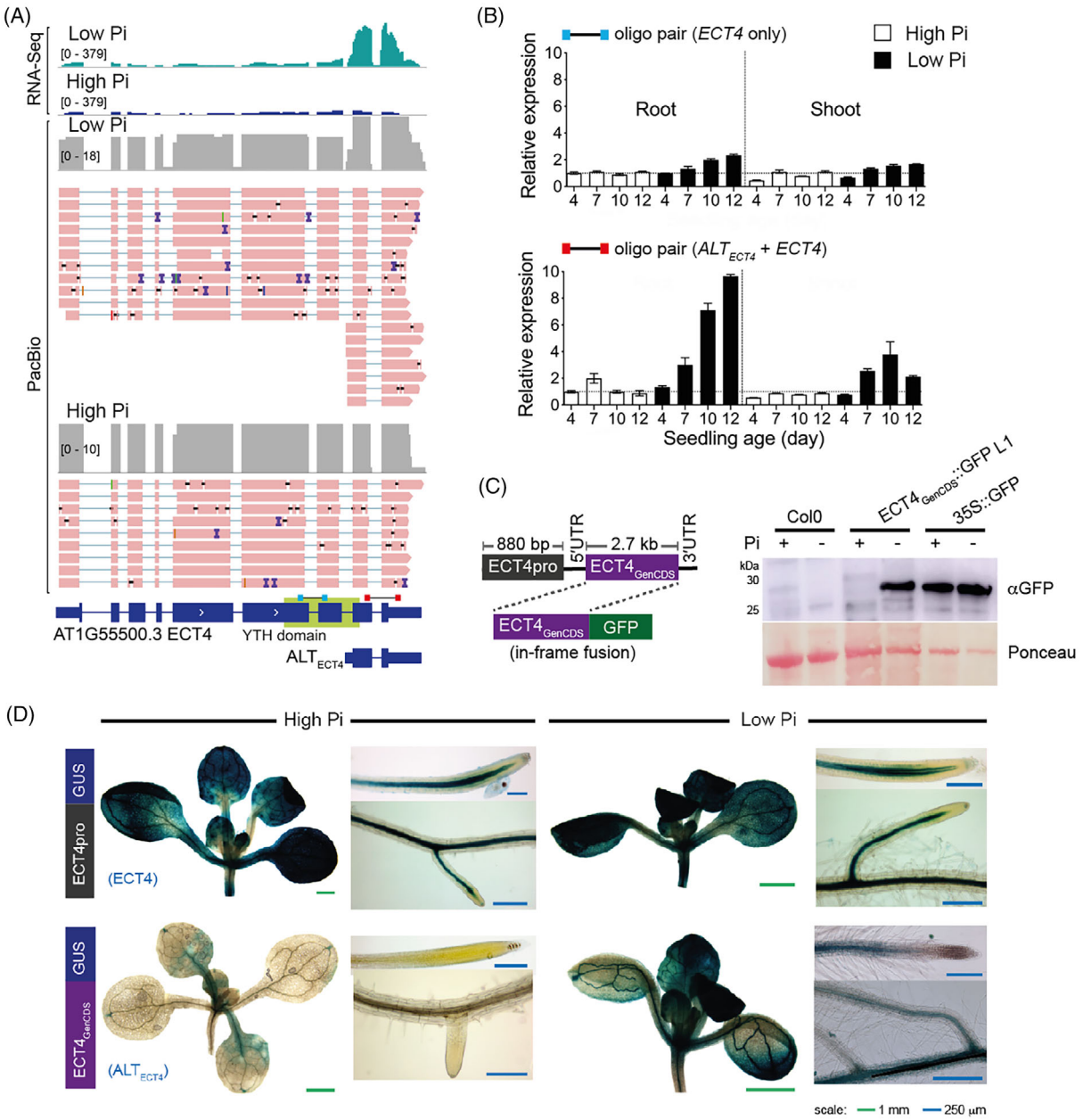

Figure 5. Pi deficiency induces alternative promoter selection associated with *ECT4*.

(A) Illumina RNA-Seq reads density graph (upper panel) and PacBio reads for full-length mRNAs (lower panel) are shown for plants grown on Pi-deficient and Pi-sufficient media. The ALT_{ECT4} sequence is depicted using the annotation for *ECT4*'s coding sequence (thickest line; bottom panel). Exons are depicted as larger filled boxes, 5′ and 3′ UTRs as thinner filled boxes, and introns as lines, with the direction of transcription indicated by arrows.

(B) Time course of *ECT4* and ALT_{ECT4} expression in plants grown on Pi-sufficient and Pi-deficient media. Reverse transcription–quantitative PCR (RT–qPCR) using oligo pairs [see (A), bottom panel for the positions of the oligos] specific to *ECT4* (top panel) or both *ECT4* and ALT_{ECT4} (bottom panel); RT–qPCR experiments were repeated at least three times.

(C) *GFP* expression driven by the ALT_{ECT4} promoter. The ALT_{ECT4} promoter includes ~2.7 kb of the *ECT4* coding sequence ($ECT4_{GenCDS}$) from the start codon (ATG) to the penultimate codon fused in frame to *GFP* and expressed as a transgene in a stably transformed line (L1). Free GFP control extracted from transgenic plants expressing *GFP* under the CaMV 35S promoter as well as extracts from untransformed Col-0 were used. Protein extracts were made from 7-day-old plants grown under Pi-sufficient (+) and Pi-deficient (−) media.

(D) Promoter-GUS staining profile using the 880 bp *ECT4* promoter region (*ECT4pro*) or the ALT_{ECT4} promoter ($ECT4_{GenCDS}$) in tissues of plants grown on Pi-sufficient and Pi-deficient media. For all main panels: shoot (left), primary root (upper right), and lateral root(s) (lower right) are shown. Scale bars represent either 1 mm (green) or 250 μm (blue).

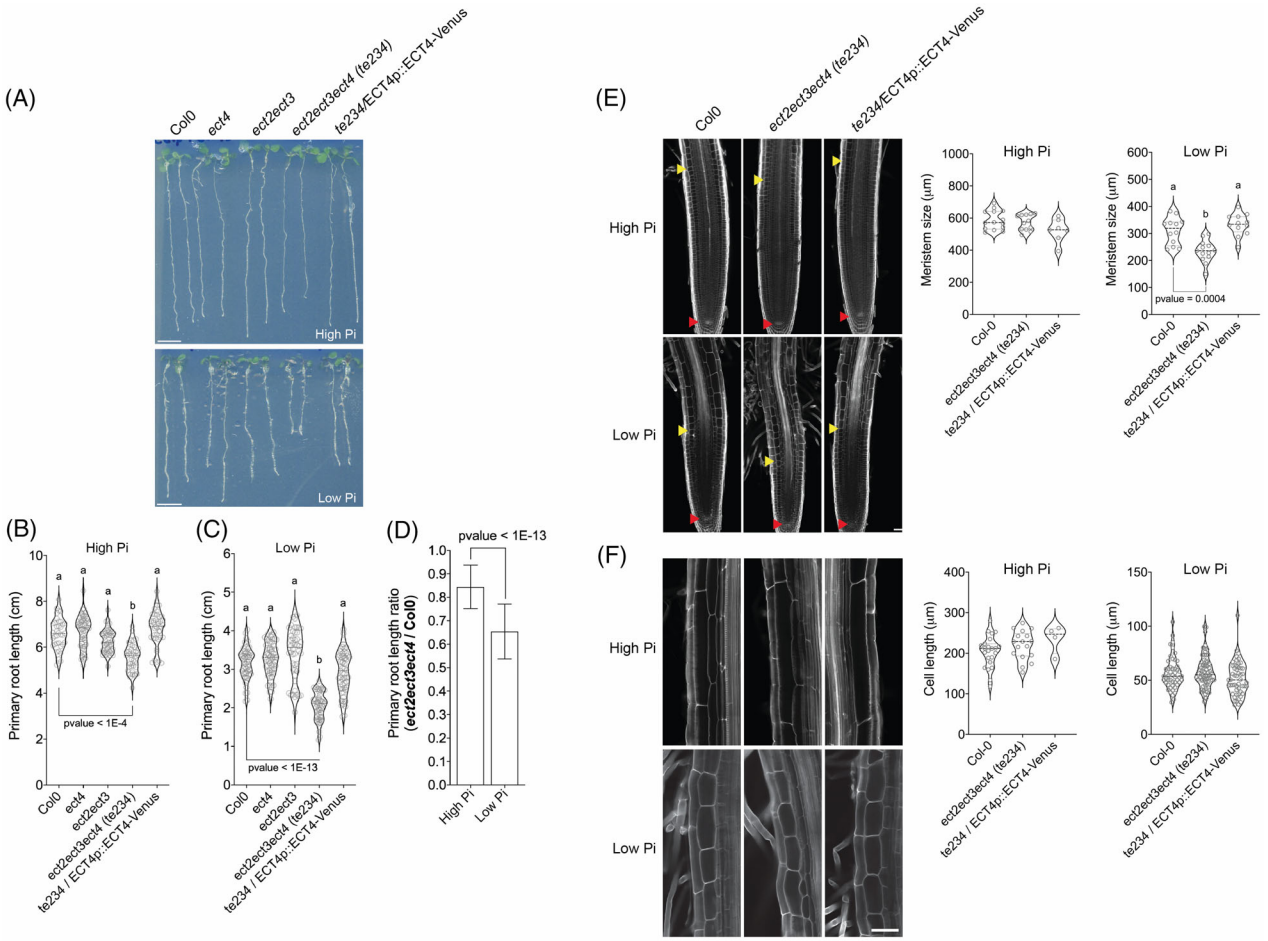

Figure 6. ECT m^{6}A readers are involved in primary root development in response to Pi deficiency.
(A–D) Primary root length of plants grown on Murashige and Skoog (MS) plates for 10 days. Representative plants of each genotype (A) and primary root length [(B, C); one-way ANOVA; $n > 30$ biological replicates] are shown. Primary root length ratios of the *ect2 ect3 ect4* triple mutant versus the wild type under control (1 mM Pi) and Pi deficiency (10 µM Pi) conditions (*t*-test, $n > 30$ biological replicates) are shown in (D).
(E, F) Size of the cell division zone in the meristem, defined in (E) by the yellow and red arrows, and cell length in the differentiation zone (F). Statistical analysis (E, F) was performed by two-way ANOVA followed by a Tukey's test; significant differences compared to Col-0 under each growth condition are indicated by lowercase letters on the graphs. Scale bar: 1 mm (A) and 50 µm (E, F).

dependent on the presence of iron (Fe) in the growth medium (Balzergue et al., 2017; Mora-Macías et al., 2017; Müller et al., 2015). Indeed, we determined that the enhanced reduction in primary root growth observed in the *te234* mutant versus the wild type was dependent on Fe in the medium (Figure 7A–C). We visualized Fe localization and accumulation in roots using Perls-DAB staining (Figure 7D; Figure S6). Under both high- and low-Pi conditions, the *te234* mutant accumulated more Fe in the meristematic and elongation zone of the root compared to both wild-type and complemented plants. The strongest Fe accumulation occurred in the root differentiation zone of the *te234* mutant under low-Pi conditions compared to both wild-type and complemented plants. Together, these results indicate that m^{6}A readers play a role in modulating primary root meristematic activity in response to low Pi in an Fe-dependent manner.

CONCLUDING REMARKS

Transcript isoform diversity can arise from alternative TSS usage, splicing, or transcript termination. Alternative TSS usage is an important mechanism that can modulate post-transcriptional regulation and protein localization and function (de Klerk & 't Hoen, 2015; Forrest et al., 2014; Kurihara et al., 2018; Thieffry et al., 2022; Ushijima et al., 2017; Wang et al., 2019). However, much less is known about its role in generating noncoding transcripts. Our study revealed that alternative TSS usage is specifically regulated by Pi starvation at many gene loci, some of which (e.g., *RTNLB1*, *HY1*, and *SQD2*) might encode proteins

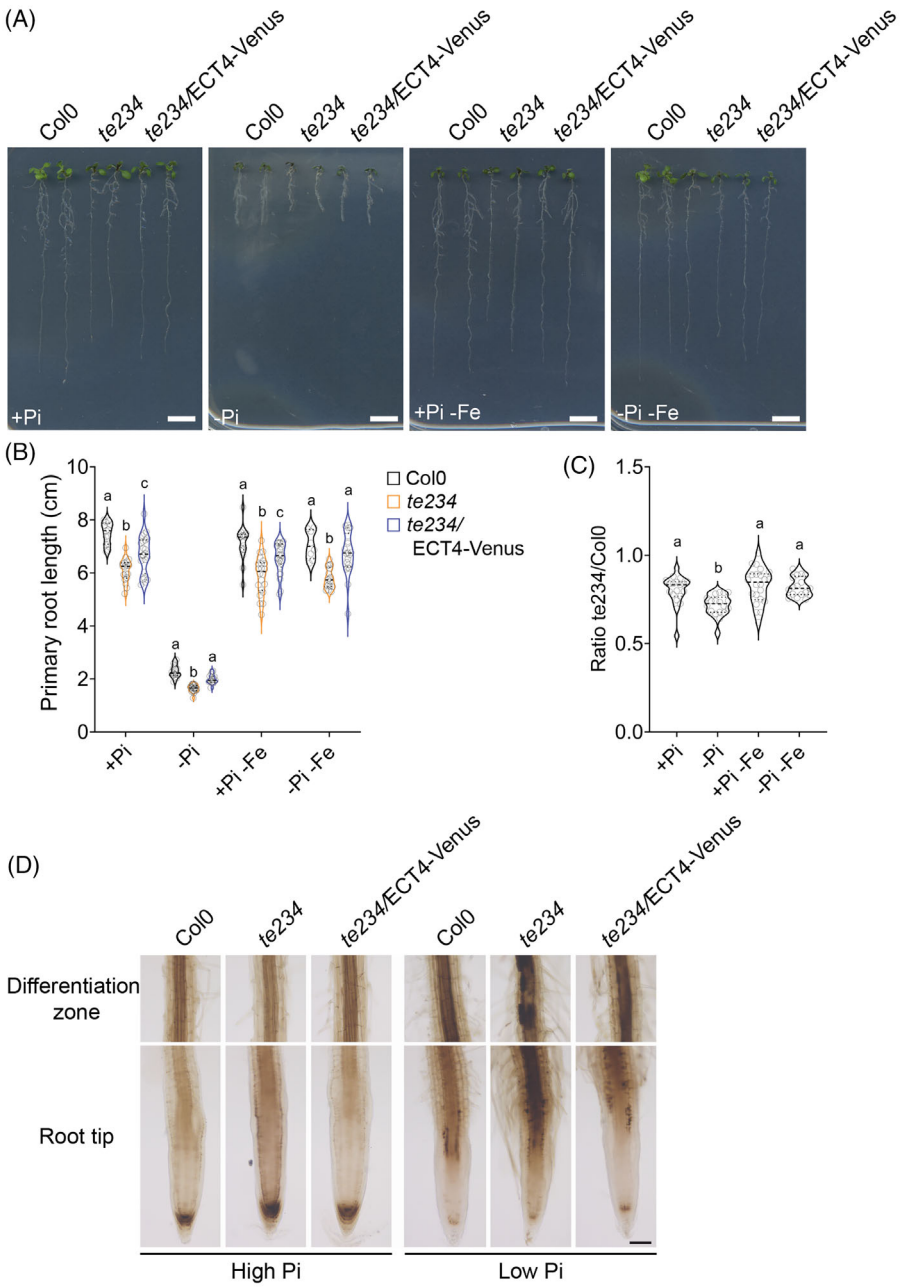

Figure 7. The *ect2 ect3 ect4* (*te234*) triple mutant shows reduced primary root growth under Pi deficiency.
(A–C) Primary root length of plants grown on MS plates for 10 days. Representative plants of each genotype (A) and primary root length [(B); one-way ANOVA; $n > 30$ biological replicates] are shown. Primary root length ratios of the *ect2 ect3 ect4* triple mutant versus the wild type under control conditions (*t*-test, $n > 30$ biological replicates) are shown in (C). High phosphate (1 mM Pi; +Pi), Pi deficiency (10 μM Pi; −Pi), Fe deficiency (medium lacking Fe; −Fe), and a combination of conditions. For B and C, different letters indicate significant differences ($P < 0.05$).
(D) Fe accumulation and distribution in the roots of mutants grown under high- and low-Pi conditions. Plants were grown for 7 days on plates containing 1 mM or 10 μM Pi and subjected to Perls-DAB staining for Fe visualization. Scale bars in (A, D) represent 1 cm and 1 mm, respectively.

involved in mechanisms that help plants adapt to Pi deficiency, such as ER autophagy and protection from ROS. We further demonstrated that Pi deficiency regulates the production of novel noncoding RNAs via the use of alternative TSS, as shown for the ALT_{ECT4} transcript at the *ECT4* locus. Although the function of this noncoding ALT_{ECT4} transcript remains unknown, its discovery led us to identify a role for the m^6A pathway in regulating primary root growth upon Pi starvation. Our work unveiled various genes and molecular processes regulated by

alternative TSS usage under Pi deficiency that are still poorly understood. However, their study will likely yield important new insights into the contribution of this mechanism to the adaptation of plants to Pi deficiency.

METHODS

Plant material and constructs

All Arabidopsis plants used in this study, including mutants and transgenic plants, were in the Columbia (Col-0) background. T-DNA insertion lines *ect4-2* (*ect4*), *ect2-1*/*ect3-1* (*ect2ect3*) and *ect2-1*/*ect3-1*/*ect4-2* (*ect2ect3ect4*), as well as transgenic lines *ect4*/ECT4p::ECT4-Venus and *ect2ect3ect4*/ECT4p::ECT4-Venus, were gifts from Peter Brodersen and were previously described (Arribas-Hernández et al., 2018). The *ECT4* promoter region [880 upstream of the *ECT4* TSS (Arribas-Hernández et al., 2018)], *ECT4*, and ALT_{ECT4} sequences were amplified from genomic DNA and cloned into an ENTR vector (list of oligonucleotides in Table S4). Binary constructs ECT4pro::GUS and ALT_{ECT4}pro::GUS were produced by LR cloning using pMDC163 (Curtis & Grossniklaus, 2003), and ALT_{ECT4}pro::GFP was produced by LR cloning using pMDC107 (Curtis & Grossniklaus, 2003). The promoter region of ALT_{ECT4} (i.e., ALT_{ECT4}pro; 2667 nucleotides long) was cloned as the genomic sequence of *ECT4* from its START codon up to the last codon before the STOP codon (not included).

Plant growth conditions and treatments

Plants were grown on half-strength Murashige and Skoog (MS) salts (Duchefa, Haarlem, Netherlands; M0255) containing 1% (w/v) sucrose and 0.7% (w/v) agar and cultivated at 22°C under continuous light. For experiments with variable Pi concentrations in agar, MS salts without Pi (Caisson Labs; MSP11) were supplemented with Pi buffer (pH 5.7, 93.5% w/v KH_2PO_4 and 6.5% w/v K_2HPO_4) to reach a final concentration of 1 mM or 10 μM. For nitrogen starvation, MS salts without nitrogen (Caisson Labs, Smithfield, UT, USA; MSP07) were supplemented with nitrogen to a final concentration of 3 mM (1 mM NH_4NO_3 and 1 mM KNO_3) or 0.2 mM (0.07 mM NH_4NO_3, 0.07 mM KNO_3, and 0.93 mM KCl). Sample material produced for RNA-Seq and PacBio sequencing has been described previously (Deforges, Reis, Jacquet, Sheppard, et al., 2019). In brief, wild-type Col-0 seeds were germinated in half-strength MS liquid medium containing 1 mM or 100 μM Pi using MS salts without Pi, as described above. Pi-deficient plants were harvested for total RNA extraction 7 days after germination. Plant hormone treatments were performed in standard half-strength MS medium as described above. Ten days after germination, wild-type Col-0 seedlings were flooded with a solution of half-strength MS containing 5 μM IAA, 10 μM ABA, 10 μM MeJA, or no plant hormones for the untreated control. After 3 h of incubation, roots and shoots were harvested separately (three independent biological replicates).

Root measurement, microscopy, and staining

Root length was measured using seedlings grown on vertically oriented plates. The plates were scanned on a flatbed scanner to produce image files suitable for quantitative analysis using ImageJ software (v1.44p).

Confocal microscopy was performed using a Zeiss LSM 880 confocal laser scanning microscope. Plant roots were treated with ClearSee solution and stained with calcofluor white (Ursache et al., 2018) to visualize cell walls.

Roots were stained for GUS activity as previously described (Lagarde et al., 1996). The tissues were vacuum infiltrated to enhance tissue penetration. Stained tissues were cleared in chloral hydrate solution (2.7 g ml^{-1} in 30% glycerol) and analyzed under a Leica DM5000B bright-field microscope.

Iron accumulation in seedlings was assayed by Perls-DAB staining as previously described (Müller et al., 2015). Briefly, seedlings were incubated in 4 ml of 2% (v/v) HCl and 2% (w/v) potassium ferrocyanide for 30 min. The samples were washed with water and incubated for 45 min in 4 ml of 10 mM NaN_3 and 0.3% H_2O_2 in methanol. The samples were washed with 100 mM Na-phosphate buffer (pH 7.4) and incubated for 30 min in the same buffer containing 0.025% (w/v) DAB and 0.005% (v/v) H_2O_2. Finally, the samples were washed twice with water, cleared with chloral hydrate (1 g ml^{-1}, 15% v/v glycerol), and analyzed under an optical microscope.

RNA-seq and JunctionSeq analysis

The RNA-Seq dataset was previously published (Deforges, Reis, Jacquet, Sheppard, et al., 2019). Here, we applied JunctionSeq analysis (Hartley & Mullikin, 2016) to all RNA-Seq reads mapped against TAIR10 annotated genes. JunctionSeq was set to analyze differential exons only, and thus splice junctions were excluded, with a false discovery rate (FDR) of 0.01.

TeloPrime cDNA library preparation and PacBio sequencing

The same RNA extracted from plants was used for RNA-Seq (see above) and PacBio long-read analysis. A TeloPrime Full-Length cDNA Amplification Kit (Lexogen, Vienna, Austria) was used to generate full-length cDNA from 1 μg of total RNA by the Genomic Technology Facility at the University of Lausanne. Briefly, first-strand cDNA synthesis was initiated using a 3′ oligo-dT anchoring primer (RP: 5′-TCTCAGGCGTTTTTTTTTTTTTTTTT-3′) and generated by reverse transcription. The cDNA:RNA hybrid molecules were column purified and ligated to the double-stranded linker (cap-dependent linker ligation) carrying a 5′ C overhang, thus allowing base pairing with the G nucleotide of the 5′ mRNA CAP. The ligation products were again column purified, and the resulting eluted fragments were converted to full-length double-stranded cDNA by second-strand cDNA synthesis.

PacBio library preparation and sequencing in a Pacific Biosciences Sequel system were performed by the Genomic Technology Facility at the University of Lausanne. PacBio consensus sequences were obtained from subreads using CSS v4.1.0 (https://github.com/PacificBiosciences/ccs). Since first-strand cDNA synthesis was initiated using a 3′ oligo-dT anchoring primer (RP: 5′-TCTCAGGCGTTTTTTTTTTTTTTTTT-3′), the orientation of the consensus sequence was established by detecting the presence of an "AGGCGTTTT" sequence within the first 50 nucleotides of the consensus sequence (indicating that it was a reverse complement sequence) or the presence of a "AAAACGCCT" within the last 50 nucleotides of the consensus sequence (indicating that it was properly oriented). Full-length sequences were selected by detecting the presence of a "CTCACTATAG" within the first 100 nt of oriented sequences. Full-length sequences were mapped against the Arabidopsis genome (TAIR10) using minimap2 v2.17-r954-dirty with the option -ax splice:hq --seed 11 -t24 --secondary=no -r300k. Forward- and reverse-oriented sequences were used to detect potential alternative TSS between Pi starvation and control conditions. For both conditions, more than half of the sequenced cells generated a circular consensus sequence (CCS), i.e., 282 768 and 266 909 CSSs from a total of 510 489 and 520 022 sequenced

cells under Pi starvation and control conditions, respectively. The orientations of full-length CCS sequences with 5′ caps and poly-A tails were evenly split between forward and reverse sequences. The 5′ end differences of full-length transcripts (annotated full-length, truncated, and exon-skipped exon) between the low and high Pi conditions were compared using a chi-squared test uncorrected for low counts or FDR. Data S1 reports genes displaying different 5′ ends within either the 5′ UTR ($P < 0.05$) or the coding region ($P < 0.1$).

Protoplast transfection and luminescence analysis

DNA fragments encompassing the *RTNLB1* short (i.e., ALT_{RTNLB1}) 5′ UTR, the long (i.e., *RTNLB1*) 5′ UTR, as well as a mutated version of the long 5′ UTR (*RTNLB1* Δ *uORF*) where ATG codons in uORFs were mutated to ATT, were all cloned upstream of the nano luciferase gene expressed under the control of the Arabidopsis *RGS1-HXK1 INTERACTING PROTEIN 1* (*RHIP1*) promoter into the plasmid pNF_RHIP1pro (Table S1). This plasmid also contains the firefly luciferase gene under the control of the *RIBOSOMAL PROTEIN 5A* (*RPS5A*) promoter, which is used for normalization.

Arabidopsis protoplasts were produced and transformed with the various constructs as previously described (Yoo et al., 2007). In brief, wild-type Col-0 plants were grown in short photoperiod (8 h light and 16 h dark at 21°C) for 4–5 weeks and leaves were cut with razor blades to produce 0.5–1 mm leaf strips. These were submerged in enzyme solution (1% cellulase, 0.25% macerozyme, 0.4 M mannitol, 20 mM KCl, 20 mM MES and 10 mM $CaCl_2$), vacuum infiltrated, and incubated at room temperature for 2 h. Protoplasts were harvested by centrifugation at 100 ***g*** for 3 min, washed with W5 solution (154 mM NaCl, 125 mM $CaCl_2$, 5 mM KCl and 2 mM MES) and resuspended in MMG solution (4 mM MES, pH 5.7, 0.4 M mannitol, and 15 mM $MgCl_2$) at 1×10^6 protoplast ml^{-1}. Protoplast transformation was performed by combining ~1.5×10^5 protoplasts, 5 μg of plasmid, and PEG solution (40% PEG 4000, 0.2 M mannitol and 100 mM $CaCl_2$). After replacing PEG solution with W5 solution by consecutive washings, protoplasts were kept in the dark for approximately 16 h at 21°C. Transformed protoplasts were harvested by centrifugation at 6000 ***g*** for 1 min, and resuspended in 1× Passive Lysis buffer (Promega, Madison, WI, USA; E1941). The lysate was used for luminescence quantification using Nano-Glo® Dual-Luciferase® Reporter Assay System (Promega; N1610). Luminescence produced by nano luciferase was normalized for loading using that produced by firefly luciferase.

RNA isolation, RT–qPCR, and 5′ RACE analysis

Total RNA for RT–qPCR analysis was extracted from roots, shoots, and seedlings using an RNA purification kit, as described by the manufacturer (Jena Bioscience, Jena, Germany; PP-210), followed by DNase I treatment. cDNA was synthesized from 0.5 μg RNA using M-MLV Reverse Transcriptase (Promega; M3681) and oligo $d(T)_{15}$ following the manufacturer's instructions. qPCR analysis was performed using SYBR Select Master Mix (Applied Biosystems, Waltham, MA, USA; 4472908) with primer pairs specific to genes of interest and *ACT2*, which was used for data normalization. Primer sequences are listed in Table S4. Analysis of TSS by 5′ RACE was performed using a SMARTer® RACE 5′/3′ Kit (Takara, Shiga, Japan) as described in the manufacturer's protocol.

Western blot analysis

Whole 7-day-old seedlings were harvested, grounded in liquid nitrogen and mixed with protein extraction buffer (500 mM Tris-HCl pH 7.5, 150 mM NaCl, 10% [v/v] glycerol, 0.1% [v/v] NP-40, 1× Roche cOmplete™ Protease Inhibitor Cocktail). Samples were centrifuged at 14 000 ***g*** for 10 min, the supernatant was recovered, and protein concentration was determined by Bradford assay. For protein separation, protein samples were mixed with 4× Loading Buffer (4% [w/v] sodium dodecyl-sulfate [SDS], 160 mM Tris-HCl, pH 8.5, 40% [v/v] glycerol, 2 mM EDTA) to a final concentration of 1×. Sixty micrograms of total protein of Col0 and $ECT4_{GenCDS}$::GFP samples, and 15 μg of the 35S::GFP samples, were heated at 70°C for 10 min and loaded in a 4–12% gradient SDS-PAGE gel. Proteins were transferred to a polyvinylidene fluoride membrane for 1 h at 100 V, followed by blocking in phosphate-buffered saline buffer (PBST) containing 1% (w/v) BSA for 1 h. The membrane was incubated with a1:500 dilution of anti-GFP antibody (Santa Cruz Biotechnology, Dallas, TX, USA; sc-8334) in PBST 1% (w/v) BSA for 2–3 h, followed by incubation with goat anti-rabbit IgG-horseradish peroxidase-coupled secondary antibody (Santa Cruz Biotechnology; sc-2004) at a 1:20 000 dilution in PBST 1% (w/v) BSA for 1 h before chemiluminescence-image capture using the SuperSignal™ West Femto substrate (ThermoFisher, Waltham, MA, USA; 34096).

Analysis of uORFs and prediction of domains and signal peptide sequences

For each selected transcript, one transcript sequence (Araport11) derived from a corresponding representative gene model was obtained via Sequence Bulk Download from TAIR. uORFs were defined as any ORF ≤200 nt long whose ATG START codon was located at a position ≤200 nt upstream of the start codon (ATG) in the main ORF. We translated the longest reference ORF within each transcript and used InterProScan 5 (Jones et al., 2014) to detect and predict functional domains (default parameters). Similarly, each reference amino acid sequence was used to predict signal peptides using TargetP-2.0 (Almagro Armenteros et al., 2019) (organism group, plant). For alternative transcripts, the longest ORF ending at the corresponding reference ORF's STOP codon was selected for comparative analysis.

GO analysis

Gene ontology analysis was performed using the online tool DAVID (Sherman et al., 2022), specifically the Gene Functional Classification Tool using default parameters.

AUTHOR CONTRIBUTIONS

RSR, JD, and YP conceived and designed the study. JD performed RNA-Seq and JunctionSeq analysis. JC performed GUS and Fe staining, confocal microscopy as well as some RT-qPCR analysis. DJ-V selected transgenic lines. RSR performed all other experiments, except for PacBio data analysis, performed by NG, and 5′ RACE done by YP. RSR and YP wrote the paper. All authors read and approved the final manuscript.

ACKNOWLEDGEMENTS

The authors thank Peter Brodersen, University of Copenhagen, for kindly providing us with several transgenic lines related to the *ECT* genes. PacBio sequencing was performed by the University of Lausanne Genomic Technologies Facility. This work was supported, in part, by a Swiss National Science Foundation (Schweizerische Nationalfonds) Sinergia grant (CRSII3_154471 to Y.P.) and funding from the University of Lausanne. Open access funding provided by Universite de Lausanne.

CONFLICT OF INTEREST

The authors declare no competing interests.

DATA AVAILABILITY STATEMENT

PacBio long-read data are available in the NCBI BioProject database (www.ncbi.nlm.nih.gov/bioproject) under project ID PRJNA649694.

SUPPORTING INFORMATION

Additional Supporting Information may be found in the online version of this article.

Data S1. Alternative TSS genes. Genes identified by JunctionSeq and PacBio, as well as analysis of uORF, signal peptide and domain.

Figure S1. Comparison of TSS position identified in this work (45 genes identified by both JunctionSeq and PacBio analyses) with published data, when available. Large-scale TSS dataset (Nielsen et al., 2019) and condition-specific datasets, i.e., cold (Kindgren et al., 2018) and light response (Kurihara et al., 2018; Ushijima et al., 2017), were used. The relative positions of the TSS on the Arabidopsis genome are shown as colored heatmap.

Figure S2. Gene expression from Illumina RNA-seq analysis showing alternative TSS for selected genes. Total RNA was extracted from root and shoot of hormone-treated 10-day-old seedlings grown on solid MS medium, and Pi-deficient (1 mM versus 100 μM Pi) 7-day-old seedlings grown in liquid MS medium. For each gene (a, *RTNLB1*; b, *CDKC2*; c, *ECT4*), the bottom panels show exons as filled boxes and introns as lines, with the direction of transcript indicated by arrows. The 5′ and 3′ UTRs are not shown.

Figure S3. Effect of nitrogen levels on *ECT4* and ALT_{ECT4} expression. Time course of expression profile of *ECT4* and ALT_{ECT4} in plants grown on nitrate-sufficient and nitrate-deficient media. RT–qPCR using oligo pairs that specifically only detect *ECT4* (top panel) or that detect both *ECT4* and ALT_{ECT4} transcripts (bottom panel). Experiment was repeated once with three biological replicates (one-way ANOVA).

Figure S4. Promoter-GUS staining profile using the 880 bp *ECT4* promoter region (*ECT4pro*) in primary root tip of plants grown on Pi-sufficient (high Pi) and Pi-deficient (low Pi) media.

Figure S5. Expression of phosphate starvation markers. Plants were grown on high phosphate (1 mM Pi; +Pi) or Pi deficiency (10 μM Pi; −Pi) media for 10 days before harvesting roots. Experiment was repeated once with three biological replicates (one-way ANOVA).

Figure S6. Fe accumulation and distribution in the roots of mutants grown under high and low Pi conditions as visualized following Perls-DAB staining. Staining was compared between Col-0, the *ect2 ect3 ect4* triple mutant (te234) and the te234 line complemented with the ECT4-Venus construct (E4V). Staining at the root tip and differentiation zone (DZ) of the root are shown. Scale = 100 μm.

Table S1. Sequences of wild-type and mutated 5′ UTRs of the *RTNLB1 gene*. The ATG start codons associated with uORFs are in bold while the ATG codon used to define the start of the RTNLB1 protein is underlined. The ALT_{RTNLB1} 5′ UTR is found in transcripts from plants grown under both Pi-deficient and Pi-deficient conditions while the longer *RTNLB1* 5′ UTR is found primarily in transcripts from Pi-deficient plants. *RTNLB1* Δ*uORF* is a mutated form of the wild-type *RTNLB1* 5′ UTR where all nine ATG codons associated with uORFs are mutated to ATT.

Table S2. Annotated ALT_{ECT4} sequence. ALT_{ECT4} sequence obtained from PacBio long read and presented in GeneBank format.

Table S3. Transcription start sites from transgenic lines with *GFP* inserted at the 3′ end of *ECT4* coding genomic region (ALT_{ECT4} promoter). The coding genomic region of *ECT4* from the ATG start codon to the TAA stop codon is shown, with exons in capital letters and introns in small letters. The region transcribed to generate the spliced ALT_{ECT4} transcript detected in Pi-deficient WT plants is shown in red. TSS detected in 12 independent 5′ RACE clones obtained from transgenic plants expressing GFP from the ALT_{ECT4} promoter are highlighted in green, blue or pink if they were found once, twice or three times, respectively.

Table S4. Primer list.

REFERENCES

Abel, S. (2017) Phosphate scouting by root tips. *Current Opinion in Plant Biology*, **39**, 168–177.

Almagro Armenteros, J.J., Salvatore, M., Emanuelsson, O., Winther, O., von Heijne, G., Elofsson, A. *et al.* (2019) Detecting sequence signals in targeting peptides using deep learning. *Life Science Alliance*, **2**, e201900429.

Arribas-Hernández, L., Bressendorff, S., Hansen, M.H., Poulsen, C., Erdmann, S. & Brodersen, P. (2018) An m6A-YTH module controls developmental timing and morphogenesis in Arabidopsis. *The Plant Cell*, **30**(5), 952–967.

Arribas-Hernández, L., Rennie, S., Schon, M., Porcelli, C., Enugutti, B., Andersson, R. *et al.* (2021) The YTHDF proteins ECT2 and ECT3 bind largely overlapping target sets and influence target mRNA abundance, not alternative polyadenylation. *eLife*, **10**, e72377.

Arribas-Hernández, L., Simonini, S., Hansen, M.H., Botterweg Paredes, E., Bressendorff, S., Dong, Y. *et al.* (2020) Recurrent requirement for the m6A-ECT2/ECT3/ECT4 axis in the control of cell proliferation during plant organogenesis. *Development*, **147**, dev189134.

Balzergue, C., Dartevelle, T., Godon, C., Laugier, E., Meisrimler, C., Teulon, J.-M. *et al.* (2017) Low phosphate activates STOP1-ALMT1 to rapidly inhibit root cell elongation. *Nature Communications*, **8**, 15300.

Bazin, J., Baerenfaller, K., Gosai, S.J., Gregory, B.D., Crespi, M. & Bailey-Serres, J. (2017) Global analysis of ribosome-associated noncoding RNAs unveils new modes of translational regulation. *Proceedings of the National Academy of Sciences of the United States of America*, **114**, E10018–E10027.

Cartolano, M., Huettel, B., Hartwig, B., Reinhardt, R. & Schneeberger, K. (2016) cDNA library enrichment of full length transcripts for SMRT long read sequencing. *PLoS One*, **11**, 1–10.

Cheng, C., Krishnakumar, V., Chan, A.P., Thibaud-Nissen, F., Schobel, S. & Town, C.D. (2017) Araport11: a complete reannotation of the *Arabidopsis thaliana* reference genome. *The Plant Journal*, **89**, 789–804.

Cruz-Ramírez, A., Oropeza-Aburto, A., Razo-Hernández, F., Ramírez-Chávez, E. & Herrera-Estrella, L. (2006) Phospholipase DZ2 plays an important role in extraplastidic galactolipid biosynthesis and phosphate recycling in Arabidopsis roots. *Proceedings of the National Academy of Sciences of the United States of America*, **103**, 6765–6770.

Curtis, M.D. & Grossniklaus, U. (2003) A gateway cloning vector set for high-throughput functional analysis of genes in plants. *Plant Physiology*, **133**, 462–469.

Davis, S.J., Kurepa, J. & Vierstra, R.D. (1999) The *Arabidopsis thaliana* HY1 locus, required for phytochrome-chromophore biosynthesis, encodes a protein related to heme oxygenases. *Proceedings of the National Academy of Sciences of the United States of America*, **96**, 6541–6546.

de Klerk, E. & 't Hoen, P.A. (2015) Alternative mRNA transcription, processing, and translation: insights from RNA sequencing. *Trends in Genetics*, **31**, 128–139.

Deforges, J., Reis, R.S., Jacquet, P., Sheppard, S., Gadekar, V.P., Hart-Smith, G. *et al.* (2019) Control of cognate sense mRNA translation by cis-natural antisense RNAs. *Plant Physiology*, **180**, 305–322.

Deforges, J., Reis, R.S., Jacquet, P., Vuarambon, D.J. & Poirier, Y. (2019) Prediction of regulatory long intergenic non-coding RNAs acting in trans through base-pairing interactions. *BMC Genomics*, **20**, 601.

Dong, C., **He, F.**, **Berkowitz, O.**, **Liu, J.**, **Cao, P.**, **Tang, M.** ***et al.*** (2018) Alternative splicing plays a critical role in maintaining mineral nutrient homeostasis in rice (*Oryza sativa*). *Plant Cell*, **30**, 2267–2285.

Ebina, I., **Takemoto-Tsutsumi, M.**, **Watanabe, S.**, **Koyama, H.**, **Endo, Y.**, **Kimata, K.** ***et al.*** (2015) Identification of novel *Arabidopsis thaliana* upstream open reading frames that control expression of the main coding sequences in a peptide sequence-dependent manner. *Nucleic Acids Research*, **43**, 1562–1576.

Emborg, T.J., **Walker, J.M.**, **Noh, B.** & **Vierstra, R.D.** (2006) Multiple heme oxygenase family members contribute to the biosynthesis of the phytochrome chromophore in Arabidopsis. *Plant Physiology*, **140**, 856–868.

Essigmann, B., **Güler, S.**, **Narang, R.A.**, **Linke, D.** & **Benning, C.** (1998) Phosphate availability affects the thylakoid lipid composition and the expression of SQD1, a gene required for sulfolipid biosynthesis in *Arabidopsis thaliana*. *Proceedings of the National Academy of Sciences of the United States of America*, **95**, 1950–1955.

Forrest, A.R.R., **Kawaji, H.**, **Rehli, M.**, **Baillie, J.K.**, **De Hoon, M.J.L.**, **Haberle, V.** ***et al.*** (2014) A promoter-level mammalian expression atlas. *Nature*, **507**, 462–470.

Franco-Zorrilla, J.M., **Valli, A.**, **Todesco, M.**, **Mateos, I.**, **Puga, M.I.**, **Rubio-Somoza, I.** ***et al.*** (2007) Target mimicry provides a new mechanism for regulation of microRNA activity. *Nature Genetics*, **39**, 1033–1037.

Guo, M., **Zhang, Y.**, **Jia, X.**, **Wang, X.**, **Zhang, Y.**, **Liu, J.** ***et al.*** (2022) Alternative splicing of REGULATOR OF LEAF INCLINATION 1 modulates phosphate starvation signaling and growth in plants. *The Plant Cell*, **34**, 3319–3338.

Gutiérrez-Alanís, D., **Ojeda-Rivera, J.O.**, **Yong-Villalobos, L.**, **Cárdenas-Torres, L.** & **Herrera-Estrella, L.** (2018) Adaptation to phosphate scarcity: tips from Arabidopsis roots. *Trends in Plant Science*, **23**, 721–730.

Ham, B.-K., **Chen, J.**, **Yan, Y.** & **Lucas, W.J.** (2018) Insights into plant phosphate sensing and signaling. *Current Opinion in Biotechnology*, **49**, 1–9.

Hartley, S.W. & **Mullikin, J.C.** (2016) Detection and visualization of differential splicing in RNA-Seq data with JunctionSeq. *Nucleic Acids Research*, **44**, e127.

Hsieh, L.-C., **Lin, S.-I.**, **Kuo, H.-F.** & **Chiou, T.-J.** (2010) Abundance of tRNA-derived small RNAs in phosphate-starved Arabidopsis roots. *Plant Signaling & Behavior*, **5**, 537–539.

Jones, P., **Binns, D.**, **Chang, H.-Y.**, **Fraser, M.**, **Li, W.**, **McAnulla, C.** ***et al.*** (2014) InterProScan 5: genome-scale protein function classification. *Bioinformatics*, **30**, 1236–1240.

Jung, J.Y., **Ried, M.K.**, **Hothorn, M.** & **Poirier, Y.** (2018) Control of plant phosphate homeostasis by inositol pyrophosphates and the SPX domain. *Current Opinion in Biotechnology*, **49**, 156–162.

Kindgren, P., **Ard, R.**, **Ivanov, M.** & **Marquardt, S.** (2018) Transcriptional read-through of the long non-coding RNA SVALKA governs plant cold acclimation. *Nature Communications*, **9**, 4561.

Knox, K., **Wang, P.**, **Kriechbaumer, V.**, **Tilsner, J.**, **Frigerio, L.**, **Sparkes, I.** ***et al.*** (2015) Putting the squeeze on plasmodesmata: a role for reticulons in primary plasmodesmata formation. *Plant Physiology*, **168**, 1563–1572.

Kurihara, Y., **Makita, Y.**, **Kawashima, M.**, **Fujita, T.**, **Iwasaki, S.** & **Matsui, M.** (2018) Transcripts from downstream alternative transcription start sites evade uORF-mediated inhibition of gene expression in Arabidopsis. *Proceedings of the National Academy of Sciences of the United States of America*, **115**, 7831–7836.

Lagarde, D., **Basset, M.**, **Lepetit, M.**, **Conejero, G.**, **Gaymard, F.**, **Astruc, S.** ***et al.*** (1996) Tissue-specific expression of Arabidopsis AKT1 gene is consistent with a role in K+ nutrition. *The Plant Journal*, **9**, 195–203.

Lee, H.Y., **Bowen, C.H.**, **Popescu, G.V.**, **Kang, H.G.**, **Kato, N.**, **Ma, S.** ***et al.*** (2011) Arabidopsis RTNLB1 and RTNLB2 reticulon-like proteins regulate intracellular trafficking and activity of the FLS2 immune receptor. *Plant Cell*, **23**, 3374–3391.

Li, D., **Zhang, H.**, **Hong, Y.**, **Huang, L.**, **Li, X.**, **Zhang, Y.** ***et al.*** (2014) Genome-wide identification, biochemical characterization, and expression analyses of the YTH domain-containing RNA-binding protein family in Arabidopsis and Rice. *Plant Molecular Biology Reporter*, **32**, 1169–1186.

Li, W., **Lin, W.-D.**, **Ray, P.**, **Lan, P.** & **Schmidt, W.** (2013) Genome-wide detection of condition-sensitive alternative splicing in Arabidopsis roots. *Plant Physiology*, **162**, 1750–1763.

Mahawar, L. & **Shekhawat, G.S.** (2018) Haem oxygenase: a functionally diverse enzyme of photosynthetic organisms and its role in phytochrome chromophore biosynthesis, cellular signalling and defence mechanisms. *Plant, Cell & Environment*, **41**, 483–500.

Misson, J., **Raghothama, K.G.**, **Jain, A.**, **Jouhet, J.**, **Block, M.A.**, **Bligny, R.** ***et al.*** (2005) A genome-wide transcriptional analysis using *Arabidopsis thaliana* Affymetrix gene chips determined plant responses to phosphate deprivation. *Proceedings of the National Academy of Sciences of the United States of America*, **102**, 11934–11939.

Mora-Macías, J., **Ojeda-Rivera, J.O.**, **Gutiérrez-Alanís, D.**, **Yong-Villalobos, L.**, **Oropeza-Aburto, A.**, **Raya-González, J.** ***et al.*** (2017) Malate-dependent Fe accumulation is a critical checkpoint in the root developmental response to low phosphate. *Proceedings of the National Academy of Sciences of the United States of America*, **114**, E3563–E3572. Available from: https://doi.org/10.1073/pnas.1701952114

Müller, J., **Toev, T.**, **Heisters, M.**, **Teller, J.**, **Moore, K.L.**, **Hause, G.** ***et al.*** (2015) Iron-dependent callose deposition adjusts root meristem maintenance to phosphate availability. *Developmental Cell*, **33**, 216–230.

Naumann, C., **Müller, J.**, **Sakhonwasee, S.**, **Wieghaus, A.**, **Hause, G.**, **Heisters, M.** ***et al.*** (2019) The local phosphate deficiency response activates endoplasmic reticulum stress-dependent autophagy. *Plant Physiology*, **179**, 460–476.

Nielsen, M., **Ard, R.**, **Leng, X.**, **Ivanov, M.**, **Kindgren, P.**, **Pelechano, V.** ***et al.*** (2019) Transcription-driven chromatin repression of intragenic transcription start sites. *PLoS Genetics*, **15**, e1007969.

Nziengui, H., **Bouhidel, K.**, **Pillon, D.**, **Der, C.**, **Marty, F.** & **Schoefs, B.** (2007) Reticulon-like proteins in *Arabidopsis thaliana*: structural organization and ER localization. *FEBS Letters*, **581**, 3356–3362.

Péret, B., **Clément, M.**, **Nussaume, L.** & **Desnos, T.** (2011) Root developmental adaptation to phosphate starvation: better safe than sorry. *Trends in Plant Science*, **16**, 442–450.

Poirier, Y., **Jaskolowski, A.** & **Clúa, J.** (2022) Phosphate acquisition and metabolism in plants. *Current Biology*, **32**, R623–R629.

Prall, W., **Ganguly, D.R.** & **Gregory, B.D.** (2023) The covalent nucleotide modifications within plant mRNAs: what we know, how we find them, and what should be done in the future. *The Plant Cell*, **35**, 1801–1816.

Reis, R.S., **Deforges, J.**, **Sokoloff, T.** & **Poirier, Y.** (2020) Modulation of shoot phosphate level and growth by PHOSPHATE1 upstream open reading frame. *Plant Physiology*, **183**, 1145–1156.

Reyes, A. & **Huber, W.** (2018) Alternative start and termination sites of transcription drive most transcript isoform differences across human tissues. *Nucleic Acids Research*, **46**, 582–592.

Roy, E.D., **Richards, P.D.**, **Martinelli, L.A.**, **Coletta, L.D.**, **Lins, S.R.M.**, **Vazquez, F.F.** ***et al.*** (2016) The phosphorus cost of agricultural intensification in the tropics. *Nature Plants*, **2**, 16043.

Sattari, S.Z., **Bouwman, A.F.**, **Martinez Rodríguez, R.**, **Beusen, A.H.W.** & **van Ittersum, M.K.** (2016) Negative global phosphorus budgets challenge sustainable intensification of grasslands. *Nature Communications*, **7**, 10696.

Shao, Y., **Wong, C.E.**, **Shen, L.** & **Yu, H.** (2021) N6-methyladenosine modification underlies messenger RNA metabolism and plant development. *Current Opinion in Plant Biology*, **63**, 102047.

Shekhawat, G.S. & **Verma, K.** (2010) Haem oxygenase (HO): an overlooked enzyme of plant metabolism and defence. *Journal of Experimental Botany*, **61**, 2255–2270.

Sherman, B.T., **Hao, M.**, **Qiu, J.**, **Jiao, X.**, **Baseler, M.W.**, **Lane, H.C.** ***et al.*** (2022) DAVID: a web server for functional enrichment analysis and functional annotation of gene lists (2021 update). *Nucleic Acids Research*, **50**, W216–W221.

Song, P., **Wei, L.**, **Chen, Z.**, **Cai, Z.**, **Lu, Q.**, **Wang, C.** ***et al.*** (2023) m6A readers ECT2/ECT3/ECT4 enhance mRNA stability through direct recruitment of the poly(A) binding proteins in Arabidopsis. *Genome Biology*, **24**, 103.

Srivastava, A.K., **Lu, Y.**, **Zinta, G.**, **Lang, Z.** & **Zhu, J.K.** (2018) UTR-dependent control of gene expression in plants. *Trends in Plant Science*, **23**, 248–259.

Tarkowski, Ł.P., **Signorelli, S.**, **Considine, M.J.** & **Montrichard, F.** (2023) Integration of reactive oxygen species and nutrient signalling to shape root system architecture. *Plant, Cell & Environment*, **46**, 379–390.

Teufel, F., **Almagro Armenteros, J.J.**, **Johansen, A.R.**, **Gíslason, M.H.**, **Pihl, S.I.**, **Tsirigos, K.D.** ***et al.*** (2022) SignalP 6.0 predicts all five types of signal peptides using protein language models. *Nature Biotechnology*, **40**, 1023–1025.

Thieffry, A., **López-Márquez, D.**, **Bornholdt, J.**, **Malekroudi, M.G.**, **Bressendorff, S.**, **Barghetti, A.** ***et al.*** (2022) PAMP-triggered genetic reprogramming involves widespread alternative transcription initiation and an immediate transcription factor wave. *The Plant Cell*, **34**, 2615–2637.

Tian, P., **Lin, Z.**, **Lin, D.**, **Dong, S.**, **Huang, J.** & **Huang, T.** (2021) The pattern of DNA methylation alteration, and its association with the changes of gene expression and alternative splicing during phosphate starvation in tomato. *The Plant Journal*, **108**, 841–858.

Ursache, R., **Andersen, T.G.**, **Marhavý, P.** & **Geldner, N.** (2018) A protocol for combining fluorescent proteins with histological stains for diverse cell wall components. *The Plant Journal*, **93**, 399–412.

Ushijima, T., **Hanada, K.**, **Gotoh, E.**, **Yamori, W.**, **Kodama, Y.**, **Tanaka, H.** ***et al.*** (2017) Light controls protein localization through phytochrome-mediated alternative promoter selection. *Cell*, **171**, 1–10.

Wang, K., **Wang, D.**, **Zheng, X.**, **Qin, A.**, **Zhou, J.**, **Guo, B.** ***et al.*** (2019) Multi-strategic RNA-seq analysis reveals a high-resolution transcriptional landscape in cotton. *Nature Communications*, **10**, 4714.

Wu, H.-Y.L., **Ai, Q.**, **Teixeira, R.T.**, **Nguyen, P.H.T.**, **Song, G.**, **Montes, C.** ***et al.*** (2024) Improved super-resolution ribosome profiling reveals prevalent translation of upstream ORFs and small ORFs in Arabidopsis. *The Plant Cell*, **36**, 510–539.

Yoo, S.-D., **Cho, Y.-H.** & **Sheen, J.** (2007) Arabidopsis mesophyll protoplasts: a versatile cell system for transient gene expression analysis. *Nature Protocols*, **2**, 1565–1572.

Yu, B., **Xu, C.** & **Benning, C.** (2002) Arabidopsis disrupted in SQD2 encoding sulfolipid synthase is impaired in phosphate-limited growth. *Proceedings of the National Academy of Sciences of the United States of America*, **99**, 5732–5737.

Zhan, X., **Shen, Q.**, **Chen, J.**, **Yang, P.**, **Wang, X.** & **Hong, Y.** (2019) Rice sulfoquinovosyltransferase SQD2.1 mediates flavonoid glycosylation and enhances tolerance to osmotic stress. *Plant, Cell & Environment*, **42**, 2215–2230.

Zhan, X., **Shen, Q.**, **Wang, X.** & **Hong, Y.** (2017) The sulfoquinovosyltransferase-like enzyme SQD2.2 is involved in flavonoid glycosylation, regulating sugar metabolism and seed setting in rice. *Scientific Reports*, **7**, 4685.

Zhang, R., **Kuo, R.**, **Coulter, M.**, **Calixto, C.P.G.**, **Entizne, J.C.**, **Guo, W.** ***et al.*** (2022) A high-resolution single-molecule sequencing-based Arabidopsis transcriptome using novel methods of iso-seq analysis. *Genome Biology*, **23**, 149.

Zhang, X., **Ding, X.**, **Marshall, R.S.**, **Paez-Valencia, J.**, **Lacey, P.**, **Vierstra, R.D.** ***et al.*** (2020) Reticulon proteins modulate autophagy of the endoplasmic reticulum in maize endosperm. *eLife*, **9**, e51918.

Zhang, Z., **Liao, H.** & **Lucas, W.J.** (2014) Molecular mechanisms underlying phosphate sensing, signaling, and adaptation in plants. *Journal of Integrative Plant Biology*, **56**, 192–220.